Modeling assessment of storm surge in the Salish Sea

Zhaoqing Yang[1,2]*, Taiping Wang[1], Luca Castrucci[3] and Ian Miller[4]

[1]Marine Sciences Laboratory, Pacific Northwest National Laboratory, Seattle, WA, USA
[2]Department of Civil and Environmental Engineering, University of Washington, Seattle, WA, USA
[3]Formerly with Pacific Northwest National Laboratory, Seattle, WA, USA
[4]Washington Sea Grant, University of Washington, Seattle, WA, USA

*Corresponding author: zhaoqing.yang@pnnl.gov

ABSTRACT

This paper presents a modeling assessment of storm surge in the Salish Sea—a large and complex estuarine system in the Pacific Northwest that is exposed to extratropical cyclones. A method was developed to systematically identify storm surge events in the Salish Sea based on water level records at four representative tidal gauges in the Salish Sea. The maximum storm surge distribution in the Salish Sea was calculated based on model simulations of 34 major historical storm events from 1980 to 2016. The model simulations were validated by field observations of water level and velocity using a suite of model performance metrics. Model results suggest that the maximum storm surge in the Salish Sea is generally in the range of 0.8 m to 1.03 m and is heterogeneous in space. The model results also show a strong north-south gradient with larger surge magnitudes occurring in the north that is primarily caused by the southerly wind in winter months. The sensitivity analysis with wind forcing suggested that storm surge in the Salish Sea is dominated by the remote surge from the Pacific Ocean, and the local wind contributes up to approximately 20% of the surge variability. This paper systematically elucidates storm surge characteristics and potential risk in the Salish Sea.

Keywords: storm surge; Salish Sea; modeling; windstorm; assessment

1. Introduction

Storm surge is one of the most dangerous natural threats to many coastal regions around the world (Hauer et al. 2016; Mousavi et al. 2011; Nicholls and Cazenave 2010; Soontiens et al. 2016; Tebaldi et al. 2012). The Pacific Northwest (PNW) coast of North America is subject to the threat of storm surge and coastal inundation induced by extratropical cyclones, which cause severe weather conditions such as high winds and heavy rainfalls (Abeysirigunawardena et al. 2009, Cheng et al. 2015, Eichler and Higgins 2006, Martin et al. 2001, Steenburgh and Mass 1996). The Salish Sea, located on the PNW coast, is one of the largest inland seas in the world, and it has complex sub-basins and interconnected waterways (Figure 1). Although the inland waterways of the Salish Sea are partially shielded from the direct attack of Pacific Ocean storms by Vancouver Island and the Olympic Peninsula, storm surge induced by the combination of PNW windstorms and localized wind effects often leads to increased water levels and coastal inundation in the Salish Sea (Thomson et al. 2009).

Coastal communities in the Salish Sea are frequently flooded because of the combination of high tides and storm surge caused by extreme weather events. Concerns about the more frequent occurrence of extreme sea levels and associated risks contributed by windstorms and waves in the Salish Sea have been increasing. To date, however, little information about storm surge in Puget Sound at fine spatial scales is available to coastal managers and planners for use in preparing shoreline protection plans and developing flood mitigation strategies. Few studies have been devoted to systematically understanding the spatial distribution of storm surge, waves, and sea level rise under extreme weather events in the Salish Sea (Abeysirigunawardena et al. 2011, Bromirski et al. 2017, Miller et al. 2018, Soontiens et al. 2016, Yang et al. 2015). Therefore, there is a strong need to accurately quantify the maximum storm surge using high-resolution coastal ocean models and to assess the potential risk of extreme sea level rise in the Salish Sea, especially in the sub-basins where nonlinear

responses could amplify storm surge magnitudes (Arns et al. 2017, Bilskie et al. 2016, Miller et al. 2018, Rego and Li 2010, Wang and Yang 2019, Yang et al. 2016, Yang et al. 2014b, Zhang et al. 2017).

However, accurately simulating storm surge in the Salish Sea poses a challenge for several reasons. First, the large tidal ranges in the Salish Sea, which can exceed 3 m, present a signal-to-noise ratio problem for quantifying the storm surge magnitudes, which are often less than 1 m. Second, having an accurate wind field with high spatiotemporal resolution is critical for storm surge model validation and predictions. Unlike the U.S. East Coast and Gulf of Mexico regions, for which high-quality reanalysis hurricane wind fields are produced by the National Oceanic and Atmospheric Administration's (NOAA's) Hurricane Research Division, no similar wind products are produced for windstorm events on the West Coast. Finally, unlike tropical cyclones and hurricanes, which are tracked by name, extratropical cyclones in the Pacific Ocean are not typically tracked by name, which makes it relatively difficult to identify storm events to simulate and evaluate the induced storm surge level on the West Coast.

This paper presents the first modeling study conducted to systematically simulate and assess the potential maximum storm surge levels in the Salish Sea at the sub-basin scale using a validated hydrodynamic model. A brief description of the study site, modeling framework, and approach is provided in Section 2. Model validation results for water levels and currents are presented in Section 3, followed by Section 4, in which the spatial variability of storm surge in the Salish Sea, especially in Puget Sound sub-basins, and the effects of wind forcing are presented. Conclusions of the study and future research needs are discussed in Section 5.

2. Methods

2.1. Study Site

The Salish Sea is a large, complex estuarine system with a large network of interconnected waterways on the PNW coast (Figure 1), which includes major waterbodies such as the Strait of Juan de Fuca (SJDF) in the west, Strait of Georgia in the north, and Puget Sound in the south. Puget Sound can be divided into four deep basins connected by shallower sills: Hood Canal, Whidbey Basin, South Sound, and the Main Basin, which is subdivided into Admiralty Inlet and the Central Basin. The tides in the Salish Sea are classified as a mixed semi-diurnal meso-tidal regime in which tidal ranges are amplified when propagating into the system from the northeast (NE) Pacific Ocean. The hydrodynamics in the Salish Sea are dominated by strong tidal currents and density-driven two-layer circulation (Babson et al. 2006, Khangaonkar et al. 2017, Lavelle et al. 1991, Sutherland et al. 2011, Yang and Wang 2013a, Yang and Khangaonkar 2010).

Water levels in the Salish Sea are monitored by a network of tidal stations operated by NOAA and Fisheries and Oceans, Canada. In 2015, NOAA conducted a comprehensive current survey at a number of locations in the Main Basin of Puget Sound using acoustic Doppler current profilers (ADCPs). Figure 1 shows representative real-time tidal gauges inside the Salish Sea and four representative ADCP stations in the Main Basin of Puget Sound. The tide gauge data and ADCP data were used for specification of model boundary conditions and validation of the storm surge simulations in the Salish Sea.

Figure 1. Study site – the Salish Sea located on the Pacific Northwest Coast, which includes major water bodies of the SJDF, Strait of Georgia, and Puget Sound. The solid circles and triangles in the map respectively indicate the water level and ADCP survey stations used in this study. The red lines indicate the two open boundaries located near Neah Bay and Campbell River for the storm surge model.

2.2. Storm Surge Model

The storm surge model used for this study was based on the unstructured-grid, Finite-Volume Coastal Community Model (FVCOM) (Chen et al. 2003). FVCOM is a general-purpose hydrodynamic and circulation model that has been used extensively for modeling storm surge in many coastal regions worldwide (Chen et al. 2014, Li et al. 2011, Sun et al. 2013, Wang and Yang 2019, Yang et al. 2015, Zhao et al. 2010). The unstructured, flexible grid framework allows FVCOM to robustly simulate fine-scale hydrodynamic processes for complex coastal domains such as the Salish Sea.

The storm surge model configuration was leveraged from previous modeling work in the Salish Sea (Wang and Yang 2017, Yang et al. 2012, Yang and Khangaonkar 2010, Yang and Wang 2013b, Yang et al. 2014a). Figure 2a shows the model grid coverage and associated bathymetric features; e.g., the deep channels in the SDJF, Strait of Georgia, and Puget Sound Main Basin, shallow sills near Admiralty Inlet and the entrance of Hood Canal, and shallower sub-basins such as Bellingham Bay, Whidbey Basin, and South Sound. The model domain consists of approximately 120,000 nodes and 215,000 triangular elements in the horizontal plane. The grid resolution varies from ~8 km along the open boundaries to an average of 200 m in the sub-basins of Puget Sound. Examples of detailed model grids in the Dyes and Sinclair Inlets and South Sound are shown in Figure 2b, c.

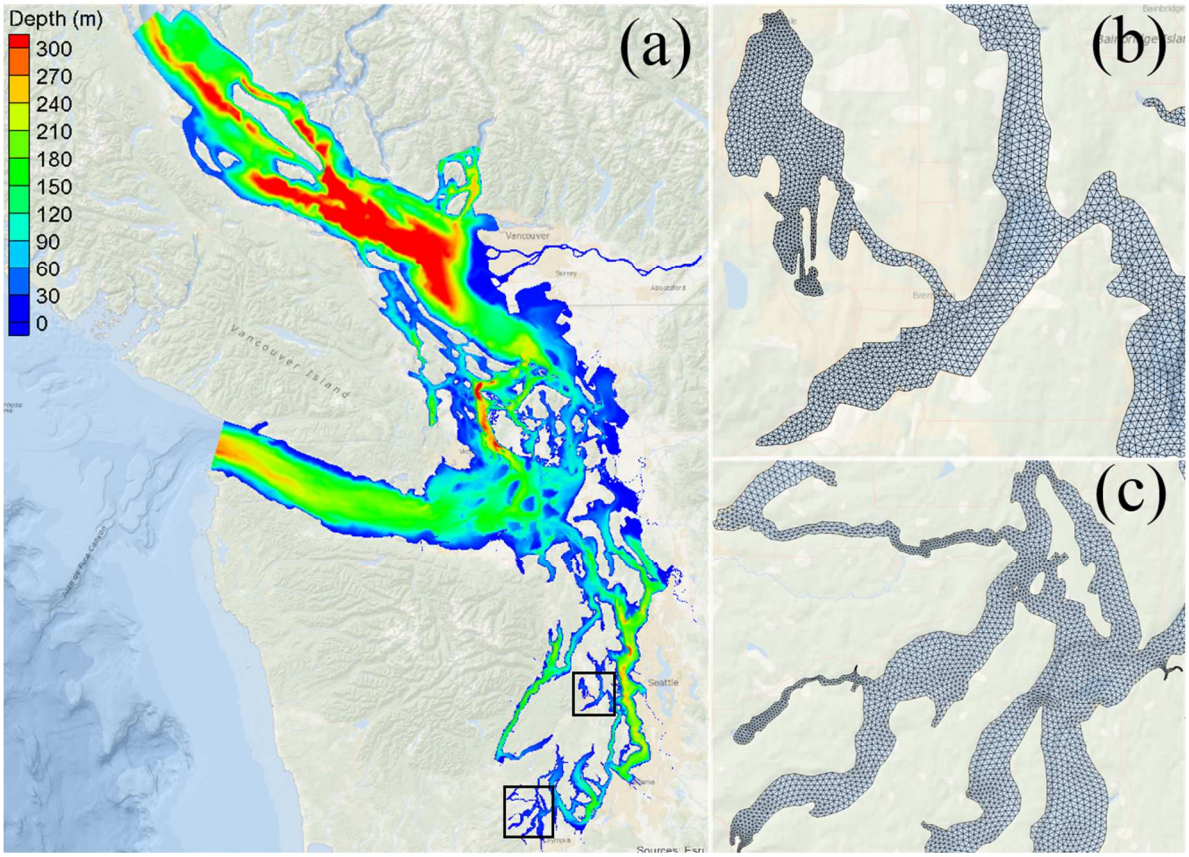

Figure 2. (a) The Salish Sea model domain and bathymetry; zoom-in model grids for (b) the Sinclair Inlet and Dyes Inlets; and (c) the multiple interconnected inlets and bays in the South Sound.

The Salish Sea storm surge model domain has two open boundaries—the eastern boundary at the entrance of SJDF and the northern boundary at the north end of the Strait of Georgia (Fig. 1). This configuration allows the model to be directly forced with observed water level data at the Neah Bay, WA, tidal gauge along the eastern open boundary and at the Campbell River, BC, tidal gauge along the northern boundary. Both tidal gauges have real-time water level observations and archived historical records. Previous studies have suggested that the storm surge inside an estuary or coastal bay is typically determined by the combination of a remote component that propagates into the system through the open boundaries and a local component generated by meteorological forcing (Liu et al. 2018,

Morey et al. 2006, Zhong et al. 2010). Therefore, by directly forcing the Salish Sea storm surge model with observed water level time series at the open boundaries, the contribution from the remote surge can be accurately captured.

Meteorological forcing, especially the wind and atmospheric pressure field, is responsible for producing local surge during storm events. In this study, the Climate Forecast System Reanalysis (CFSR) wind and atmospheric pressure field (Saha et al. 2010) of NOAA's National Centers for Environmental Prediction was used to drive the local component of the storm surge model. The CFSR wind has a spatial resolution of 0.5 degree and an hourly temporal resolution. While this spatial resolution is relatively coarse compared to the size of the storm surge model domain, the CFSR data set is still one of the best publicly available meteorological products when considering its temporal resolution (hourly) and duration (1979–present) (Wang et al. 2018). To drive the storm surge model, each time-step of the CFSR wind and atmospheric pressure were interpolated to each grid element and node, respectively.

2.3.Historical Storm Surge Events

To properly assess the maximum storm surge distribution in the Salish Sea, a sufficiently large number of simulations should be conducted based on a number of top-ranked storm surge events. However, as described in the introduction, one of the challenges for storm surge modeling in the Salish Sea is identifying storm surge events from the total water levels dominated by the large tidal range. Figure 3a shows a comparison of observed total water level and predicted tidal elevation at the NOAA real-time tide gauge at Port Aransas, TX, during 2017 Hurricane Harvey. A distinct and large storm surge induced by Hurricane Harvey is clearly seen in comparison to the water level induced by tide only. In contrast, storm surge induced by the 2006 Hanukkah Eve windstorm, one of the most destructive

storms in the modern history of the PNW, was not very evident in the observed total water level at the Seattle station, because of the effect of the large tidal range (see Figure 3b). However, once the tidal signal is removed from the total water level, i.e., by subtracting the predicted astronomical tide (red) from the measured water level (blue), the storm surge (subtidal) signal induced by the windstorm becomes more evident (Figure 3c).

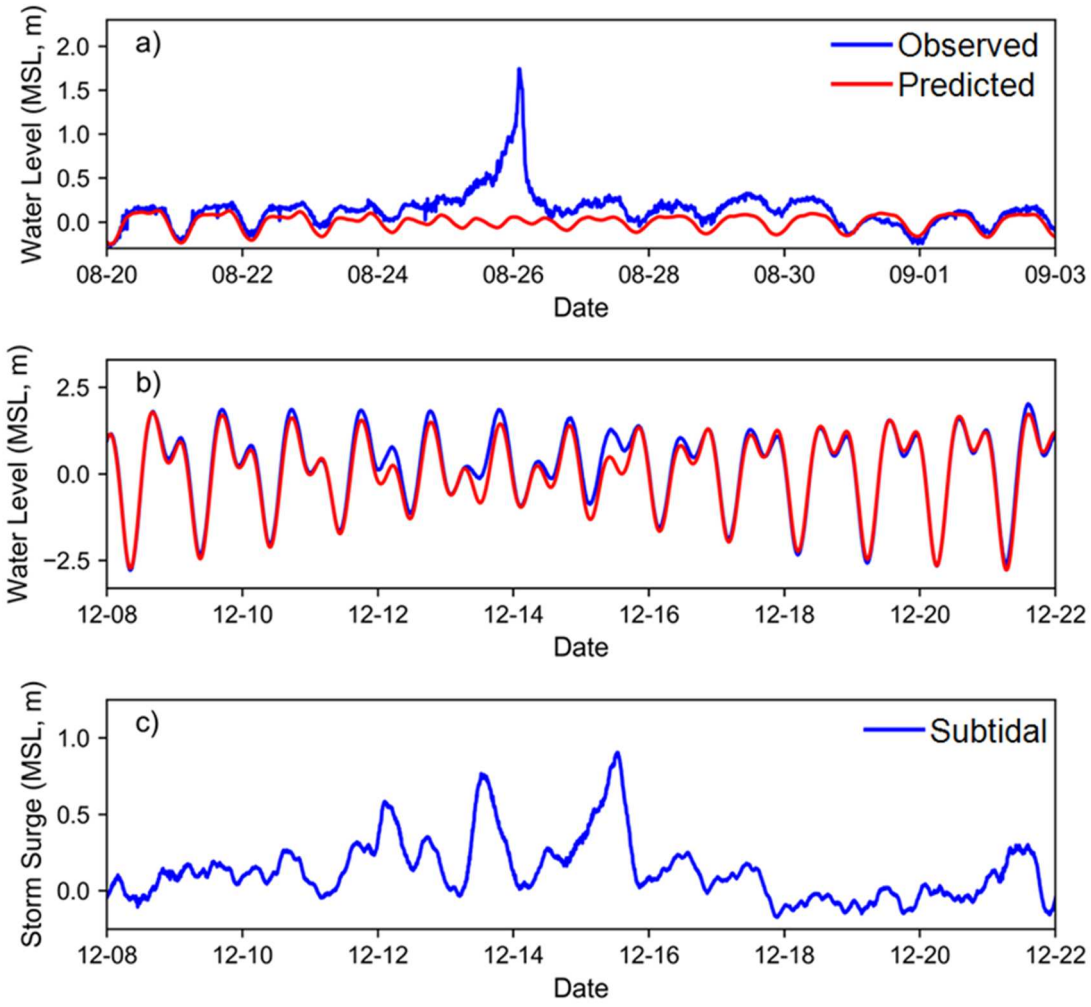

Figure 3. Comparison of the observed total water level and predicted tidal elevation at (a) Port Aransas, TX, during 2017 Hurricane Harvey; (b) the Seattle station during the 2006 Hanukkah Eve windstorm, and (c) the storm surge (subtidal) signal at the Seattle tide gauge during the 2006 Hanukkah Eve windstorm.

Subtidal water levels calculated for four spatially distributed tide gauges—Neah Bay, Port Townsend, Seattle, and Tacoma (Figure 1)—were used as the basis for identifying storm surge events for model simulation. A number of criteria were applied to those records. First, only storm events during the period from 1980 to 2016 were considered because the CFSR data are only available after 1979. Second, four NOAA tidal stations were used to identify storm surge events. Third, only storm events that had a maximum surge greater than 0.5 m across all four stations were considered. Finally, if multiple peaks over 0.5 m occurred within a 3-day window on either side of a maximum, they were all considered part of a single event, centered on the largest peak. Based on these criteria, 108 storm surge events were identified at Neah Bay, 123 at Port Townsend, 118 at Seattle, and 79 at Tacoma (see Table 1). The number of storm surge events at the Tacoma station is much less than the rest of the stations, partially because the data only became available after 1997.

Table 1. Number of identified storm surge events with storm surge values greater than 0.5 m at four NOAA real-time tide gauges.

Station	Number of Events	Data Period
Neah Bay	108	1980–2016
Port Townsend	123	1980–2016
Seattle	118	1980–2016
Tacoma	79	1997–2016

The top 20 events from each station were included. Most events were shared across tide gauges, and we selected from a list of the top 50 shared events across the four tide gauges. This led to the addition of another 14 events, for a total of 34 events. Table 2 lists the selected storm surge events in chronological order and the associated surge levels at each station. Storm surge data before 1997 at Tacoma station were not available because of the shorter tide gauge record. A flowchart illustrating the systematic approach for storm event selection and storm surge mapping based on model simulations is provided in Figure 4.

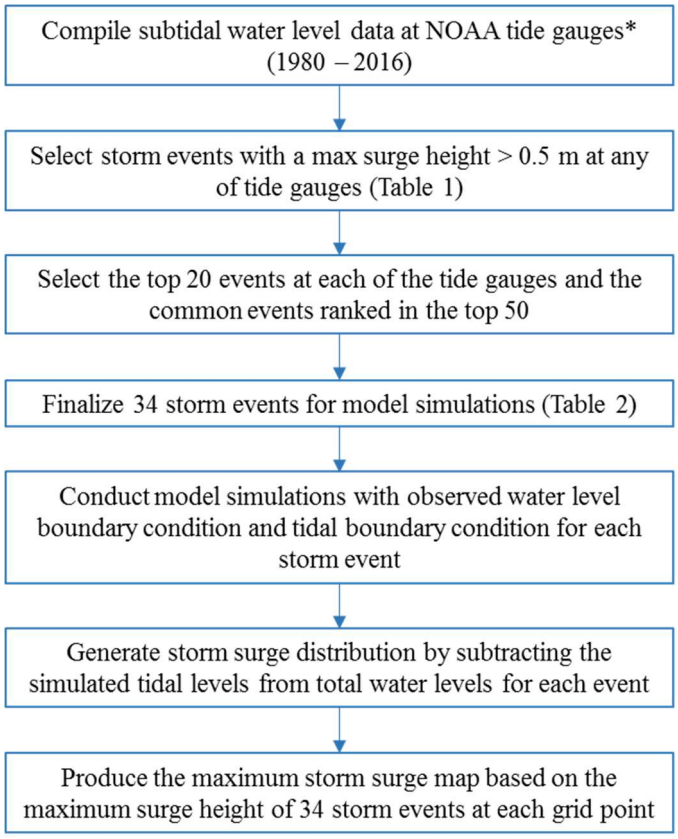

Figure 4. Systematic approach for storm event selection and final storm surge mapping in the Salish Sea. *Note: four NOAA tide gauges were used in this process – Neah Bay, Seattle, Port Townsend, and Tacoma.

211 Table 2. List of 34 selected windstorm events and the associated peak storm surge
212 magnitudes based on NOAA tide gauge data collected at the Neah Bay, Port Townsend,
213 Seattle, and Tacoma stations.

Date	Neah Bay (m)	Port Townsend (m)	Seattle (m)	Tacoma (m)
2016 - 10 - 16	0.684	0.663	0.712	0.711
2016 - 03 - 10	0.621	0.738	0.723	0.681
2016 - 03 - 06	0.518	0.749	0.709	0.720
2015 - 12 - 13	0.641	0.804	0.826	0.811
2014 - 12 - 11	0.707	0.698	0.739	0.714
2012 - 12 - 02	0.675	0.646	0.647	0.598
2010 - 01 - 18	0.660	0.751	0.760	0.796
2008 - 01 - 05	0.693	0.667	0.640	0.662
2007 - 12 - 03	0.710	0.711	0.730	0.741
2007 - 11 - 12	0.529	0.532	0.675	0.709
2006 - 12 - 15	0.651	0.797	0.901	0.886
2006 - 11 - 16	0.629	0.676	0.780	0.713
2006 - 02 - 04	0.635	0.691	0.732	0.639
2006 - 02 - 01	0.635	0.691	0.732	0.639
2002 - 12 - 16	0.814	0.804	0.794	0.848
1999 - 03 - 03	0.654	0.709	0.661	0.643
1998 - 11 - 25	0.629	0.705	0.741	0.667
1998 - 02 - 21	0.598	0.710	0.710	0.694
1998 - 02 - 12	0.659	0.637	0.637	0.627
1998 - 02 - 07	0.610	0.685	0.667	0.658
1997 - 10 - 04	0.639	0.620	0.629	0.597
1997 - 01 - 01	0.850	0.852	0.792	N/A
1996 - 02 - 21	0.669	0.530	0.551	N/A
1992 - 01 - 31	0.691	0.662	0.658	N/A
1992 - 01 - 28	0.664	0.650	0.658	N/A
1987 - 12 - 09	0.662	0.626	0.658	N/A
1987 - 12 - 01	0.654	0.685	0.722	N/A
1987 - 11 - 17	0.727	0.730	0.670	N/A
1983 - 11 - 11	0.756	0.655	0.648	N/A
1983 - 02 - 12	0.668	0.582	0.583	N/A
1983 - 01 - 27	0.860	0.858	0.754	N/A
1982 - 12 - 19	0.826	0.749	0.720	N/A
1981 - 11 - 15	0.760	0.667	0.683	N/A
1980 - 01 - 12	0.649	0.723	0.651	N/A

214
215

216 The overall objective of this study was to assess the storm surge in the Salish Sea.
217 Therefore, it was important to confirm that the 34 events listed in Table 2 were generally
218 windstorm-related because they were identified purely based on subtidal water level
219 anomalies. To confirm this, we first analyzed the observed hourly wind speed distribution at
220 National Data Buoy Center (NDBC) Buoy 46087 near the entrance of the Salish Sea

(Figure 1). Figure 5a shows that the probability distribution of wind speed at Buoy 46087 during a 3-day storm surge period is significantly larger than the wind speed for the period from 2004 to 2016. Because PNW windstorms mostly occur during winter months, the distribution of the 34 storm surge events is plotted by season in Figure 5b. Clearly, all the storm surge events occurred in the months from October to March, and the highest number of events occurred in December. Although Figure 5 indicates that the 34 storm surge events tended to be associated with high wind speed, that does not necessarily mean windstorm always produces significant storm surge, because other factors may also contribute to the surge, as discussed by Abeysirigunawardena et al. (2011), Bromirski et al. (2017), and Zhai et al. (2019).

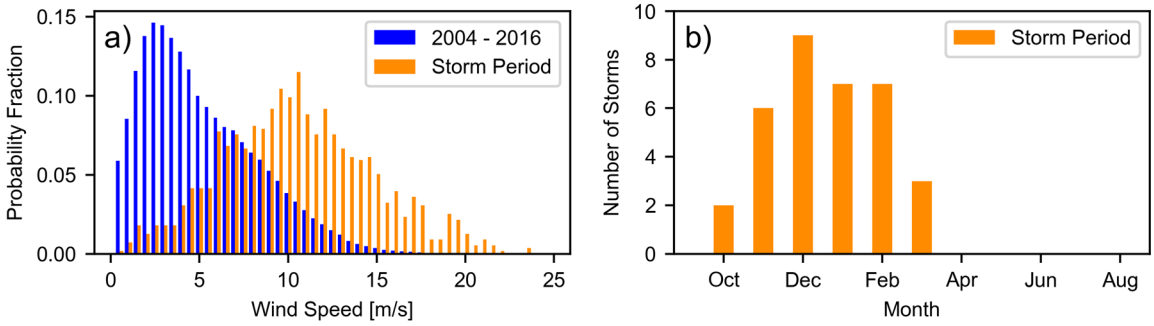

Figure 5. (a) Probability distribution of observed wind speed at NDBC Buoy 46087 for the entire data period and selected storm surge period; and (b) seasonal distribution of selected storm surge events.

2.4.Model Simulation

For each of the 34 storm surge events, paired model simulations were conducted for a 7-day window centered on the peak of the storm surge magnitude. The first model simulation for storm surge condition was forced with observed water levels, including tides, at the open boundaries and the CFSR meteorological field. The second model simulation was configured to reproduce the harmonic tides inside the model domain by forcing the model with predicted

harmonic tides at the open boundaries; i.e., the water level time series was purely constructed from 37 astronomical tidal constituents derived from long-term tidal records. Storm surge distribution in the Salish Sea was derived by subtracting the predicted water levels of tidal simulation from the storm surge simulation in the entire model domain. Time-series outputs of total water level and storm surge level were compared with observed data at all tide gauges, except at the Neah Bay station, which was used as the open boundary condition, as part of the model validation. In addition to all the storm surge model runs, a separate 20-day simulation was conducted for the period of 2015-8-20 to 2015-9-9 to evaluate the model's performance in simulating currents. Simulated tidal currents were validated against ADCP data collected by NOAA for the same period at four stations in the Main Basin and South Sound (Figure 1).

All model runs were conducted in three-dimensional and barotropic mode without considering the effect of water density variation caused by salinity and temperature. For simplicity, river discharge was not included either. Such a model configuration has been adopted as a common practice in storm surge simulation (Glahn et al. 2009), because the contribution of river discharge and density effect on water level variation is generally much more localized and smaller than that of meteorological forcing. A total of four uniform vertical layers were specified in a sigma-stretched coordinate for all the model simulations. The horizontal viscosity was calculated using Smagorinsky's eddy parameterization method (Smagorinsky 1963). The vertical viscosity was calculated using the modified Mellor and Yamada level 2.5 (MY-2.5) turbulent closure scheme (Mellor and Yamada 1982).

In FVCOM, the wind stress is calculated as:

$$\vec{\tau} = C_d \rho_a \left|\overrightarrow{U_w}\right| U_w$$

where $\vec{\tau}$ is wind stress, ρ_a is air density, $\overrightarrow{U_w}$ is wind velocity at 10 m height, and C_d is the drag coefficient as a function of wind speed (Large and Pond 1981):

$$C_d = \begin{cases} 1.2 \times 10^{-3} & \left|\overrightarrow{U_w}\right| < 11.0\ ms^{-1} \\ \left(0.49 + 0.065\left|\overrightarrow{U_w}\right|\right) \times 10^{-3} & 11.0\ ms^{-1} \le \left|\overrightarrow{U_w}\right| < 25.0\ ms^{-1} \\ (0.49 + 0.065 \times 25) \times 10^{-3} & \left|\overrightarrow{U_w}\right| > 25.0\ ms^{-1} \end{cases}$$

3. Model Results

3.1. Model Validation with Water Level

Model validation is a critical step in storm surge modeling, especially when the storm surge height in the Salish Sea is relatively small compared to the magnitude of the astronomical tides. Therefore, it is important to first verify that the model is capable of accurately simulating both total water level and storm surge. To assess the model performance, the predicted total water level and storm surge time series were compared with the observed water level and derived storm surge time series at tide gauges inside the Salish Sea for each of the 34 storm events.

Six error statistical parameters were used to quantitatively evaluate the model's capability to reproduce the water level, storm surge, and tidal current in the Salish Sea. The root-mean-square-error (*RMSE*) is defined as

$$RMSE = \sqrt{\frac{\sum_{i=1}^{N}(P_i - M_i)^2}{N}}$$

where N is the number of observations, M_i is the measured value, and P_i is the model generated value. The scatter index (*SI*) is the *RMSE* normalized by the average magnitude of measurements:

$$SI = \frac{RMSE}{abs(M)}$$

290 The mean absolute error is defined as

291 $$MAE = \frac{\sum_{i=1}^{N} abs(P_i - M_i)}{N}$$

292 The bias is defined as

293 $$Bias = \frac{\sum_{i=1}^{N} (P_i - M_i)}{N}$$

294 The percentage bias is defined as

295 $$Bias(\%) = \frac{\sum_{i=1}^{N} P_i - \sum_{i=1}^{N} M_i}{\sum_{i=1}^{N} abs(M_i)} \cdot 100$$

296 The linear correlation coefficient (*R*) is a measure of the linear relationship between the
297 predictions and the measurements from 0 to 1 where 1 corresponds to a perfect fit:

298 $$R = \frac{\sum_{i=1}^{N} \left(P_i - \overline{P}\right)\left(M_i - \overline{M}\right)}{\sqrt{\left(\sum_{i=1}^{N} \left(M_i - \overline{M}\right)^2\right)\left(\sum_{i=1}^{N} \left(P_i - \overline{P}\right)^2\right)}}$$

299 Detailed model-data comparisons for all 34 storm surge events are provided by Yang et
300 al. (2019b). As an example, only the results for one specific extreme storm event are shown
301 here. The 1996 White Christmas snowstorm hit the Salish Sea region during the 1996
302 Christmas week and caused a large storm surge inside the Salish Sea on 1997-01-01 (see
303 Table 2). Figure 6 shows the time-series comparisons of total water level and storm surge
304 height between model predictions and field measurements at the five tidal stations within the
305 model domain for the White Christmas snowstorm. The time-series comparisons for total
306 water level and storm surge heights both show excellent model-data agreement at all five
307 stations. The good model skill in simulating total water level and storm surge was confirmed
308 by the error statistics parameters summarized in Table 3for all 34 storm events. For example,
309 the *RMSE* is less than 0.1 m for the total water level at most stations—this is especially
310 encouraging considering the tidal range is about 3 m or larger in the Salish Sea. In addition,
311 the correlation coefficient (*R*) is close to one, indicating a nearly perfect linear correlation

between model predictions and observations. Comparisons of error statistics in predicted water levels indicated that the model performance in water level prediction is comparable to or better than other tidal models of the Salish Sea (Foreman et al. 2004, Soontiens et al. 2016, Sutherland et al. 2011). For storm surge height, the *RMSE* is comparable to that of total water level, while the correlation coefficient is close to 0.9. Also, the bias values for both total water level and storm surge predictions are very small (Table 3). By comparing the storm surge height and total water level time series in Figure 6, one can see that the relative timing of the maximum surge to total water level varies across different tidal stations. At Seattle station, the maximum storm surge appears to occur near high tide. Therefore, although the absolute surge height is not the highest among all the stations, the potential storm surge impact can be more pronounced, because the total water level is amplified by the contribution of tidal height.

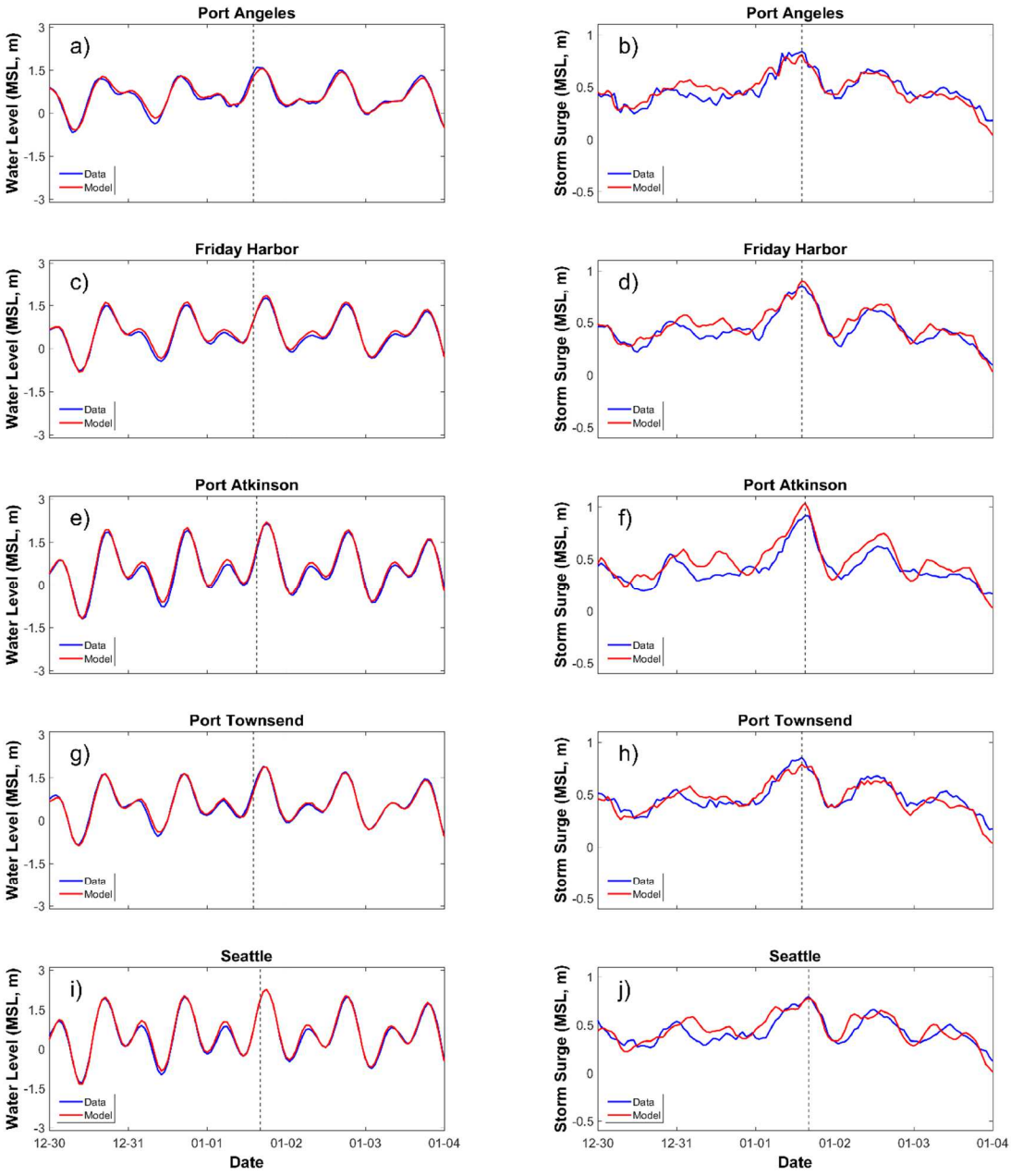

Figure 6. Comparisons of simulated and observed total water levels and storm surge heights at (a, b) Port Angeles; (c, d) Friday Harbor; (e, f) Port Atkinson; (g, h) Port Townsend, and (i, j) Seattle during the 1996 White Christmas snowstorm. The dashed line denotes the time of maximum surge observed at each tide gauge station. Tacoma station was not included because data are unavailable.

Table 3. Mean error statistics of the simulated total water level and storm surge height for all 34 storm surge events.

Station	RMSE (m)	MAE (m)	SI	Bias (m)	Bias (%)	R
Simulated Total Water Level						
Port Angeles	0.10	0.08	0.15	0.00	-0.22	0.99
Friday Harbor	0.08	0.07	0.10	0.02	1.97	0.997
Port Townsend	0.09	0.07	0.11	-0.01	-1.56	0.996
Seattle	0.09	0.08	0.09	0.03	2.67	0.998
Tacoma	0.08	0.07	0.09	0.00	0.48	0.998
Port Atkinson	0.11	0.09	0.11	0.02	1.32	0.99
Simulated Storm Surge Height						
Port Angeles	0.07	0.06	0.26	-0.02	-6.13	0.93
Friday Harbor	0.08	0.07	0.28	-0.002	-1.46	0.92
Port Townsend	0.08	0.07	0.31	-0.02	-5.39	0.91
Seattle	0.09	0.08	0.38	-0.01	-4.39	0.86
Tacoma	0.10	0.08	0.47	-0.03	-10.66	0.85
Port Atkinson	0.09	0.08	0.31	-0.04	-11.32	0.90

Moreover, it is important to evaluate the model's performance in accurately capturing the maximum surge height values observed at the tide gauges for each of the 34 storm events. Figure 7 shows the one-to-one scatterplot comparisons of the maximum surge height at the tidal gauges where water level observations for the 34 storm surge events were available. The corresponding error statistics are summarized in Table 4. Both the scatter plots and error statistics show overall good agreement between the predictions and observations of maximum storm surge values. While most of the error statistics values for simulated maximum storm surge height are comparable to those in Table 3, the linear correlation coefficient R values are lower, indicating the challenge of simulating nonlinear variability under extreme storm conditions. Overall, the good model performance metrics for total water level time series, storm surge height time series, and maximum surge height indicate the strong skill of the model to simulate the storm surge process and produce reliable results for assessing storm surge risk in the Salish Sea.

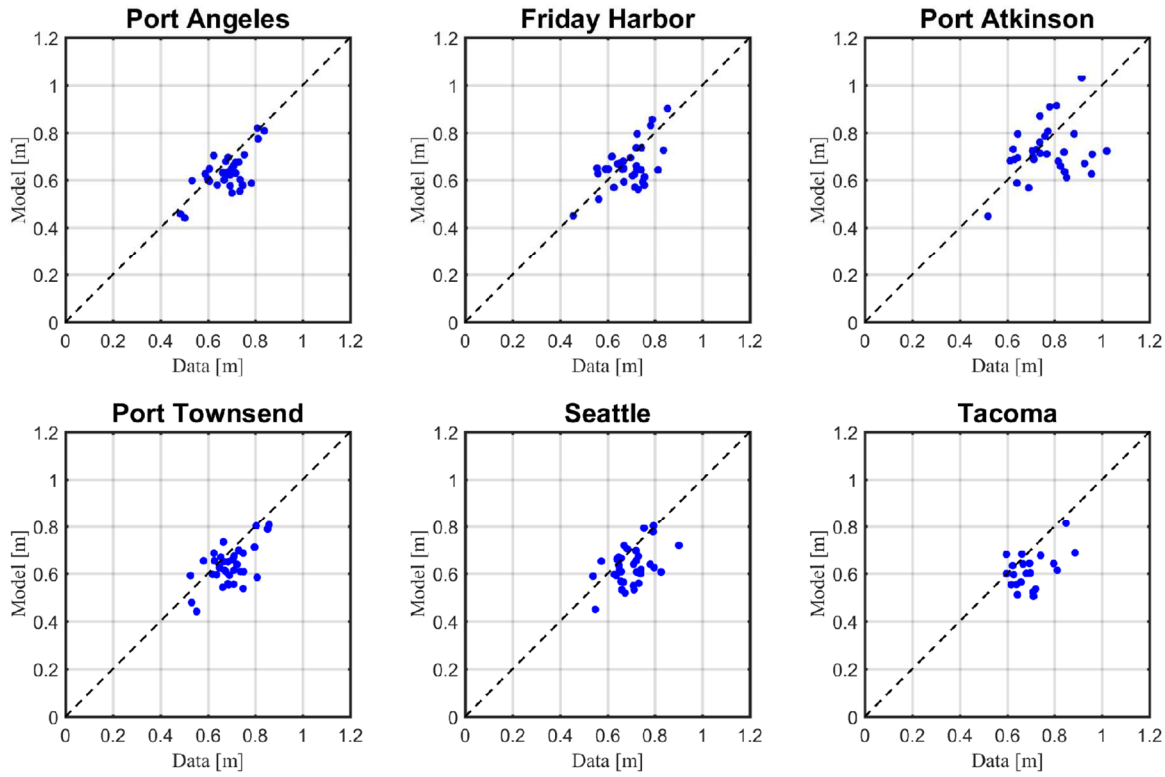

Figure 7. Scatter plots of simulated and observed maximum storm surge heights for all 34 storm surge events at six tide gauge stations in the Salish Sea. Note: there are only 21 storm surge events at Tacoma station because of the short data record.

Table 4. Mean error statistics of simulated maximum storm surge height for all 34 storm events.

Station	RMSE (m)	MAE (m)	SI	Bias (m)	Bias (%)	R
Port Angeles	0.09	0.07	0.14	-0.05	-7.76	0.64
Friday Harbor	0.09	0.07	0.13	-0.03	-4.15	0.56
Port Townsend	0.09	0.08	0.15	-0.06	-8.59	0.59
Seattle	0.10	0.08	0.16	-0.07	-9.62	0.46
Tacoma	0.12	0.09	0.19	-0.08	-12.01	0.44
Port Atkinson	0.11	0.10	0.16	-0.06	-7.31	0.56

3.2.Model Validation with Currents

To further validate the storm surge model's ability to simulate tide- and wind-driven circulation in Puget Sound, we evaluated the model's performance by comparing model-

363 simulated currents with ADCP measurements (https://cmist.noaa.gov/cmist/) at four
364 representative channel locations in the Main Basin of Puget Sound (Figure 1). The ADCP
365 data have a 6-minute temporal interval and cover a number of vertical bins throughout the
366 water column. Because the storm surge model only has four uniform vertical layers, it is more
367 meaningful to compare depth-averaged velocities. For model-data comparison, we first
368 calculated the depth-averaged East-West (U) and North-South (V) velocity components for
369 both model predictions and ADCP measurements and then projected them onto the principal
370 axis.
371
372 The time-series (principal velocity only) and scatter-point comparisons between model
373 results and ADCP data over a complete spring-neap tidal cycle are shown in Figure 8.
374 Predicted currents match the data very well at each of the four stations and the model was
375 able to successfully reproduce the spatial variability and asymmetry patterns (Figure 8). For
376 instance, currents in the deep channel of the Main Basin (PUG1511) are generally small and
377 show little tidal asymmetry (Figure 8a-b). At PUG1518 and PUG1520, located in the two
378 bifurcation channels surrounding Vashon Island, the current asymmetry shows exact opposite
379 patterns; i.e., PUG1518 is ebb-dominated (Figure 8c-d) while PUG1520 shows flood
380 dominance (Figure 8e-f). For Station PUG1526, located on the west side of Tacoma Narrows,
381 both model predictions and ADCP data show strong flood tide dominance (Figure 8g-h).
382 These tidal asymmetry patterns are largely controlled by basin geometry features. Again,
383 good error statistics of velocity predictions were achieved at all stations (Table 5). For
384 example, at PUG1526 where tidal current is strong (>2 m/s), the RMSE value is less than
385 0.15 m/s. At PUG1520 where the tidal current is very weak, error statistics are not as good as
386 they are at other ADCP stations, but they are still within the acceptable range for tidal model
387 validation. Good model-data comparisons (Figure 8) and error statistics (Table 5) confirm

that the Salish Sea storm surge model is able to accurately simulate tidal currents in Puget Sound.

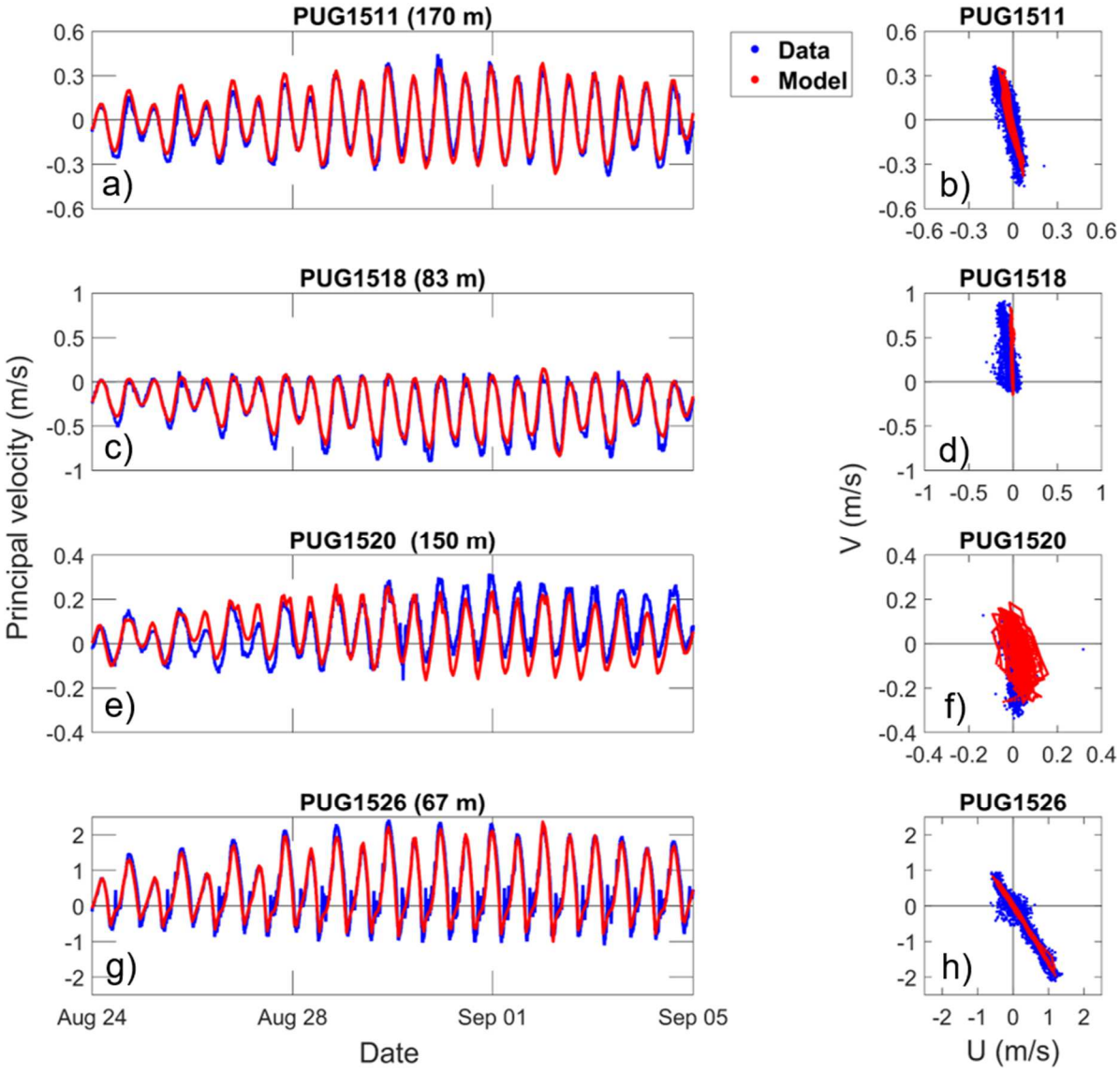

Figure 8. Comparison of simulated and observed depth-averaged velocities at PUG1511, PUG1518, PUG1520, and PUG1526 in Puget Sound (note the velocity scale changes in each plot to provide a better view of the results). The measurement period was from May 2015 to September 201 at PUG1511, and from July 2015 to September 2015 for PUG1518, PUG1520, and PUG1526.

Table 5. Error statistics for simulated tidal currents.

Station	RMSE (m/s)	MAE (m/s)	SI	Bias (m/s)	Bias%	R

PUG1511	0.04	0.03	0.25	0.00	17.24	0.84
PUG1520	0.05	0.04	0.44	0.01	24.39	0.75
PUG1518	0.06	0.05	0.24	-0.02	-7.83	0.97
PUG1526	0.14	0.11	0.22	-0.09	-12.37	0.98

4. Discussion

4.1. Spatial Variability

Figure 6 shows that the maximum storm surge height varies among tidal stations. The surge height generally ranges from 0.8 m to ~1.0 m. To assess whether the maximum surge height inside the Salish Sea can be sufficiently represented by the surge height at these tidal gauges, we calculated the maximum surge height at each model grid node and analyzed the results as a two-dimensional map. Figure 9 shows the maximum storm surge height distribution in the Salish Sea induced by the 1996 White Christmas snowstorm. Clearly, the maximum storm surge height shows distinct regional distributions. The northern portions of the Salish Sea, including the Strait of Georgia, San Juan Islands, West Sound, and North Sound, experienced the overall highest storm surge of all the major basins of the Salish Sea. For example, in the Strait of Georgia, the maximum surge height exceeds 1 m in most areas. In contrast, most of Puget Sound (e.g., the Main Basin and the majority of the South Sound) has the lowest surge height (<0.8 m), while Hood Canal and Skagit Bay experience an intermediate level of storm surge. Thus, similar to many other coastal regions, the storm surge distribution in the Salish Sea is heterogeneous in space.

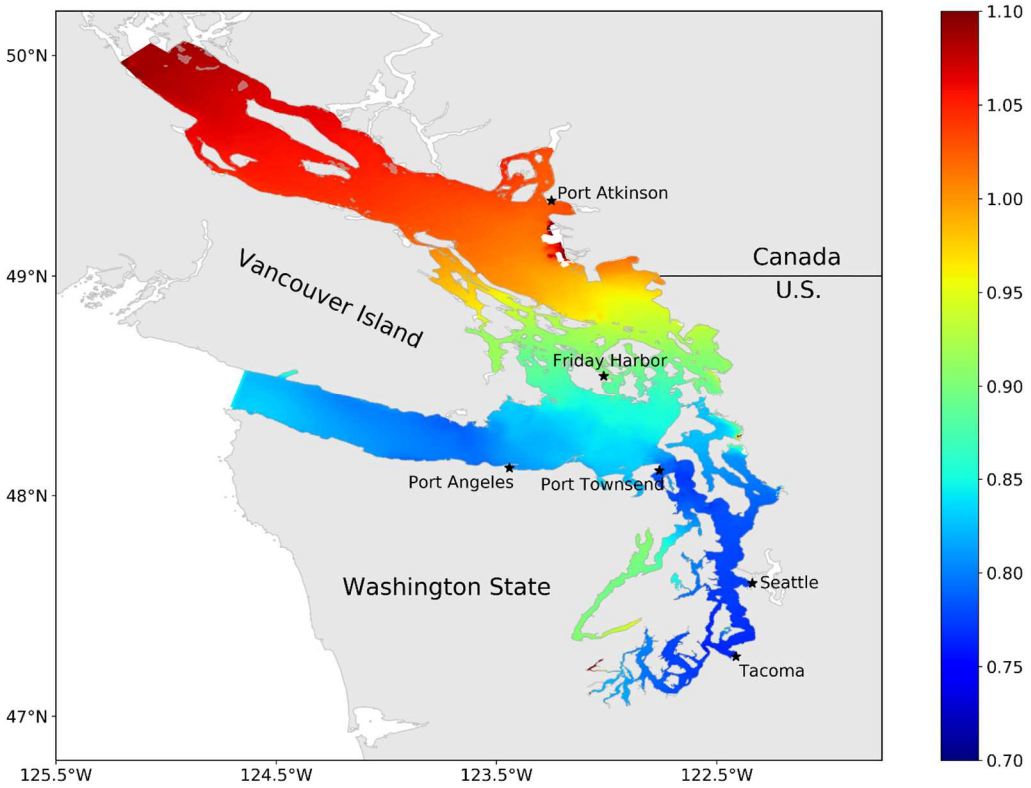

Figure 9. Simulated maximum storm surge height (m) in the Salish Sea induced by the 1996 White Christmas snowstorm.

Another major storm event—the 2006 Hanukkah Eve windstorm—shows the same spatial variability as the 1996 White Christmas snowstorm (Figure 10); e.g., higher surge in the Strait of Georgia and lower surge in the SJDF and the Main Basin, except that the range of the spatial variability is smaller than that in Figure 9. In addition, a closer comparison of Figure 9 and Figure 10 suggests that the relative difference in the maximum surge height among different basins of the Salish Sea varies between these two storms, indicating the uniqueness of maximum surge height produced by individual storm events.

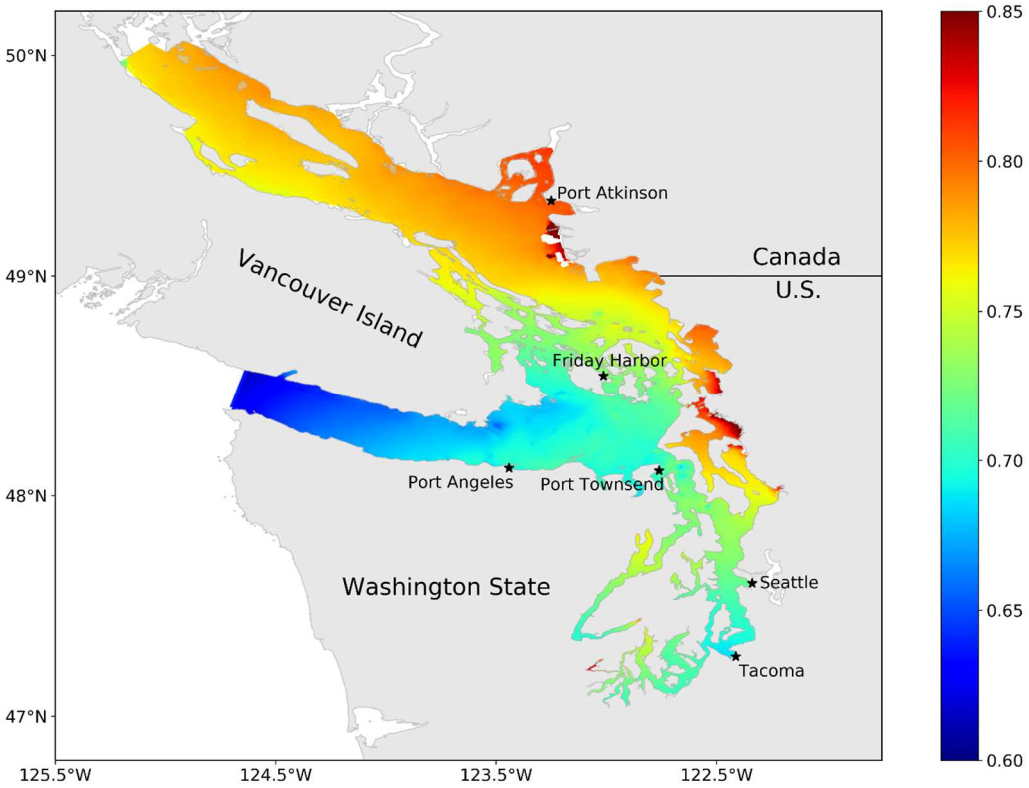

Figure 10. Simulated maximum storm surge height (m) in the Salish Sea induced by the 2006 Hanukkah Eve windstorm.

The differences between the spatial distributions of the storm surge heights of the 1997 White Christmas windstorm and the 2006 Hanukkah Eve windstorm can be illustrated by the corresponding wind fields (Figure 11). The wind patterns correlated well with model-predicted storm surge distributions for the 2006 Hanukkah Eve windstorm (Figure 9) and the 1996 White Christmas snowstorm (Figure 10). For instance, during the 1996 White Christmas windstorm, the southeasterly wind pushed the water northwestward and caused a strong setup in the north end of Georgia Strait. During the 2006 Hanukkah Eve windstorm, the dominant wind direction is from southwest. The wind pushed water toward the west and caused higher surge on the west side of the model domain, e.g., the Skagit Bay.

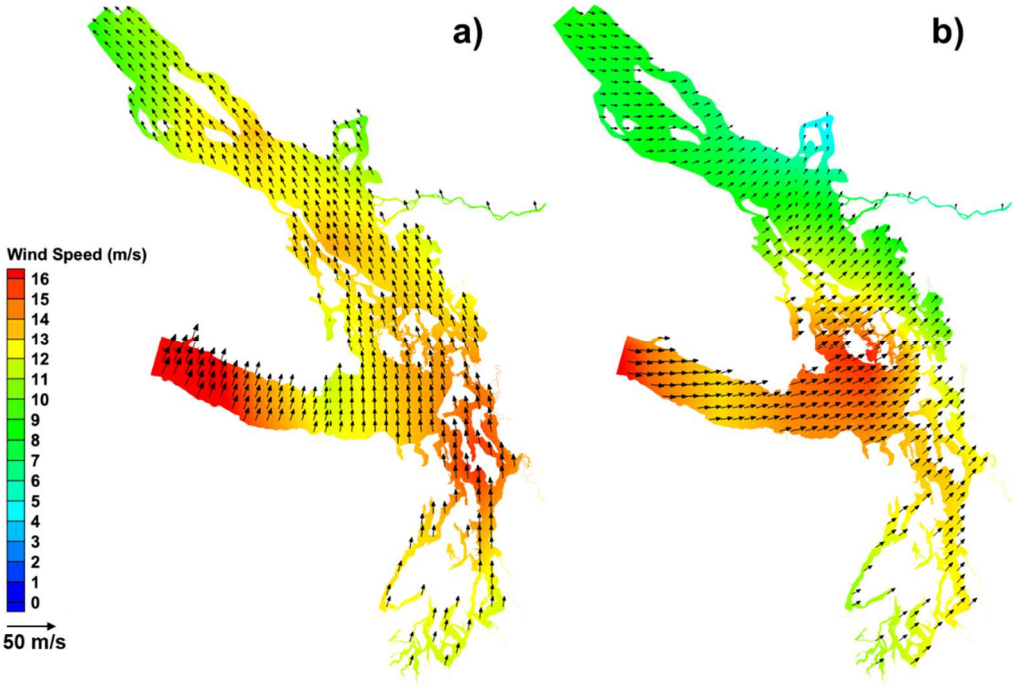

Figure 11. (a) The instantaneous (1997-1-1 11:00:00 AM) wind field for the 1997 White Christmas windstorm and (b) the instantaneous (2006-12-15 9:00:00 AM) wind field for the 2006 Hanukkah Eve windstorm.

Figure 12 shows the two-dimensional distribution of the maximum surge height compiled from all 34 storm events. The averaged maximum surge height for each sub-basin was also calculated and is presented in the figure. Again, a distinct spatial variability in the maximum surge height is seen among the individual sub-basins of the Salish Sea. The Strait of Georgia experiences the highest surge of all the basins with an average value of 1.03 m. In contrast, the Main Basin has the minimum surge height of 0.8 m. The maximum storm surge height in the SJDF also remains relatively small compared to other regions; it has an average height of 0.83 m. Interestingly, the West Sound experiences the second highest maximum surge height of all the sub-basins, which could be mainly due to its unique geometrical setting; i.e., the whole basin is connected to the Main Basin through two narrow passages (Agate Passage and Rich Passage). During storm surge events, water is being forced into the West Sound from both narrow passages, resulting in higher water level in the bay. A similar phenomenon is

also observed in the small embayment in South Puget Sound and the end of Hood Canal. In summary, these results strongly suggest that storm surge generation and propagation in the Salish Sea is a complex process, which is determined by the combination of remote surge and local surge produced by meteorological forcing and further modulated by the nonlinear interaction with basin geometry and tides.

Figure 12 also indicates that the SJDF and Main Basin in Puget Sound generally experience relatively low storm surge magnitudes—maximum surge levels are in the range of 0.80 to 0.85 m. Interestingly, the NOAA tide gauges at Port Angeles, Port Townsend, Seattle, and Tacoma are all located in the SJDF and Main Basin (Figure 1), which means that estimates of storm surge height based on water level records at these stations are accurate for the SJDF and Main Basin only, but could underestimate storm surge in other high storm surge risk sub-basins and estuaries, including Bellingham Bay in the North Sound, Hood Canal, Skagit and Port Susan Bays in Whidbey Basin, the multiple inlets in the West Sound, and very end of the South Sound.

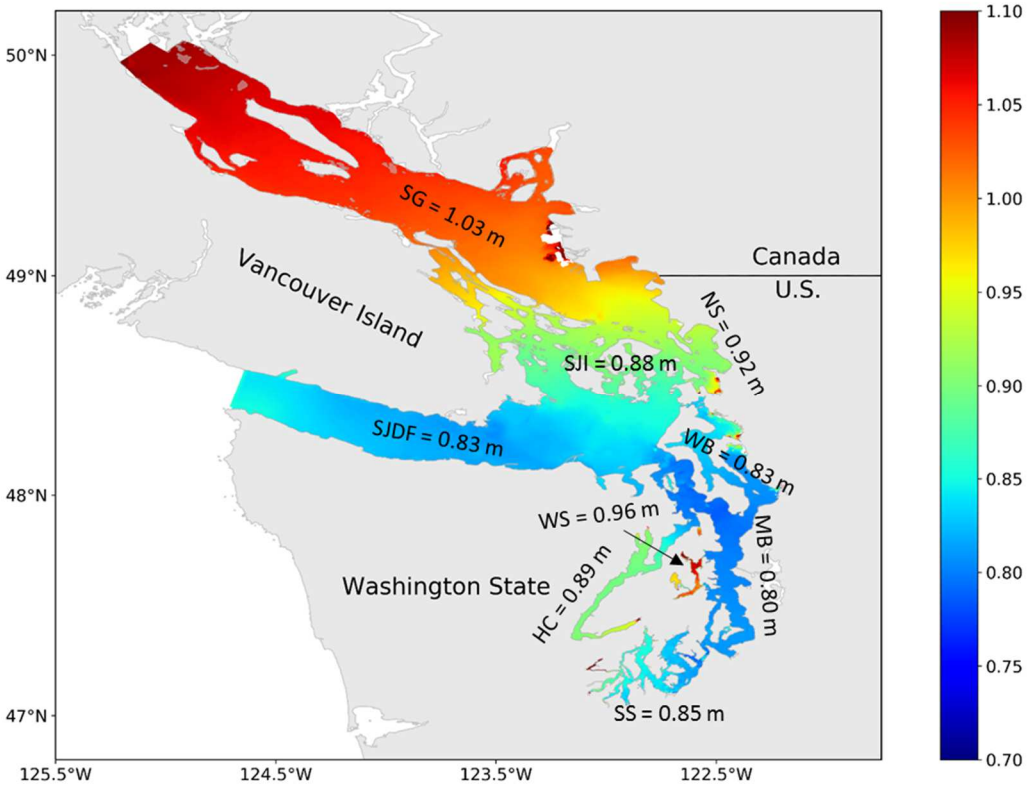

Figure 12. Distribution of maximum storm surge height (m) in the Salish Sea based on simulations of all 34 storm surge events. Values on the map indicate the mean maximum storm surge levels in the sub-basins. SJDF = Strait of Juan de Fuca; SG = Strait of Georgia; NS = North Sound; SJI = San Juan Islands; WD = Whidbey Basin; HC = Hood Canal; WS = West Sound; MB = Main Basin; SS = South Sound.

4.2. The Role of Local Wind

Storm surge inside a coastal basin is widely recognized as being largely a result of the combination of the remote surge propagated into the system from outside and the local surge generated by wind and pressure forcing inside the model domain (Liu et al. 2018, Morey et al. 2006, Zhong et al. 2010). To quantify the contribution of local meteorological forcing on the maximum surge height inside the Salish Sea, a sensitivity model run was conducted for the two most devastating windstorms—the 1996 White Christmas snowstorm and the 2006 Hanukkah Eve windstorm—by neglecting the local meteorological forcing. Specifically, in the sensitivity model runs, the model configuration remained essentially the same as that for the baseline condition, except that the wind speed and atmospheric pressure were specified as zero and standard atmospheric pressure 101,325 Pa, respectively, in both space and time. The model results for the maximum surge height were compared to those produced using meteorological forcing. The differences in the maximum surge heights at each grid node for these two storm events were calculated and are presented in Figure 13 and Figure 14, respectively. Because wind is the primary forcing to produce the local surge, the wind time series during the baseline model simulation period were also analyzed using wind rose plots for various locations throughout the model domain.

For both storm events, the results show an overall consistent spatial distribution in the change in maximum surge height; i.e., there is a distinct north-south gradient across the

model domain (Figure 13 and Figure 14). Specifically, strong south and southeast winds during both storms tend to push water northward and increase the storm surge height in the Strait of Georgia. Meanwhile, there is a reduction in the maximum surge height in the southern part of the Salish Sea. In the Salish Sea region, the wind direction is generally from south to north in winter months (Figure 13a and Figure 14a), so during windstorms, the local wind is expected to most likely contribute to increased storm surge in the northern part of the Salish Sea. In addition, the north-south gradient appeared to be larger during the 1996 White Christmas snowstorm (Figure 13b) than that during the 2006 Hanukkah Eve windstorm (Figure 14b). This is also consistent with the maximum surge height distributions shown in Figure 9 and Figure 10.

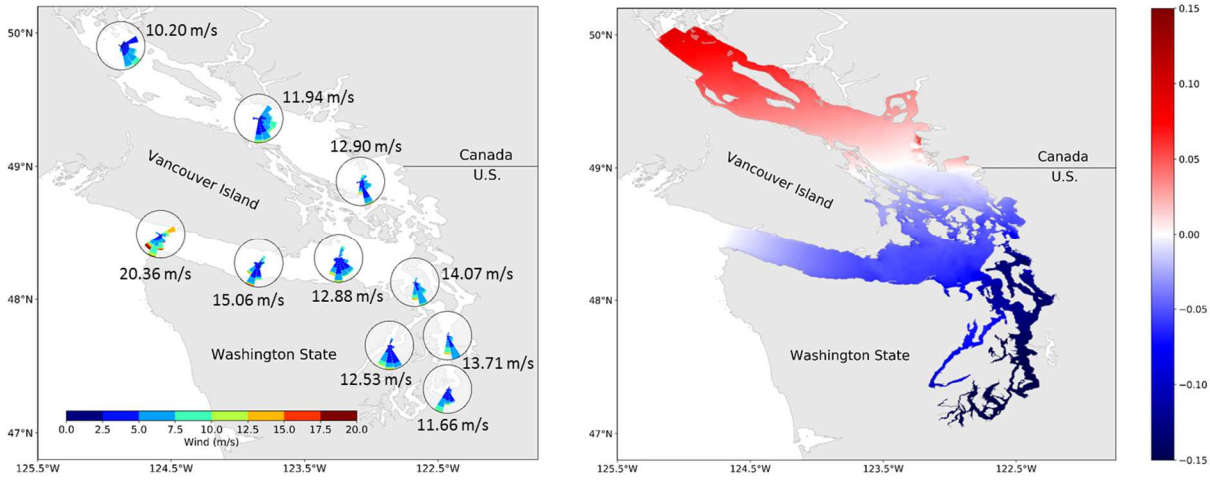

Figure 13. (a) Wind rose distribution in the Salish Sea during the 1996 White Christmas snowstorm based on CFSR wind data, and (b) the difference between simulated storm surge heights (m) with and without wind forcing. Positive value indicates areas where storm surge is underestimated when winds are not included. The value next to the wind rose denotes the maximum speed.

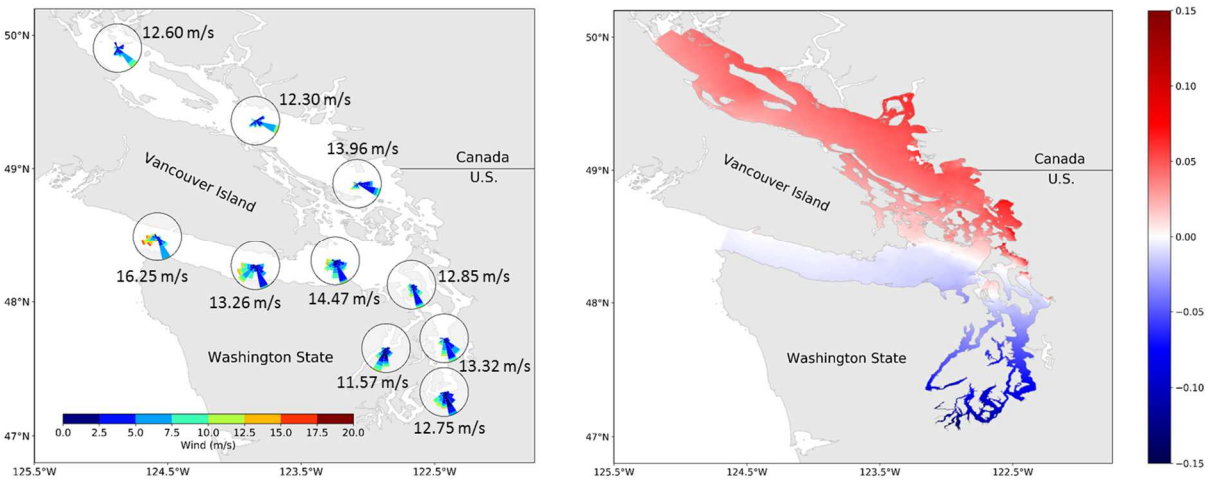

Figure 14. (a) Wind rose distribution in the Salish Sea based on CFSR wind data, and (b) the difference between simulated storm surge heights (m) with and without wind forcing during the 2006 Hanukkah Eve windstorm. Positive value indicates areas where storm surge is underestimated when winds are not included. The value next to the wind rose denotes the maximum speed.

Although the sensitivity analysis indicates that local wind results in surge setup in the northern and setdown in the southern portion of the Salish Sea, the magnitude of storm surge induced by local wind is small. For example, during the 1996 White Christmas snowstorm, the maximum (positive and negative) changes in storm surge magnitude induced by local wind were 0.09 m in Strait of Georgia and -0.18 m in South Sound, respectively. The average surge setup and setdown were 0.063 m and 0.039 m (Figure 13b). Similarly, for the Hanukkah Eve windstorm, the maximum adjustments in storm surge height by local wind were 0.08 m and -0.16 m, respectively. On average, the positive and negative adjustments were 0.037 m and -0.024 m (Figure 14b), respectively.

A sensitivity test with high-resolution wind product was also conducted to evaluate the effect of wind field resolution on the accuracy of predicted storm surge in the Salish Sea. The high-resolution wind field was based on Pacific Northwest Weather Research and Forecasting

(WRF) model simulation with a 6-km resolution (Gao et al. 2017), which was successfully applied to simulate wave climate in the Salish Sea (Yang et al. 2019a). Sensitivity runs with the high-resolution WRF wind field were conducted for two storm surge events, 2015-12-13 and 2014-12-11 (see Table 2). The results indicated that although the high-resolution wind field increased the spatial variability of storm surge distribution in the Salish Sea, the overall error statistics of storm surge height at the tidal gauges were not improved compared to those reported in Table 3. A similar study of the effect of wind field resolution by Soontiens et al. (2016) also showed that the high-resolution wind did not improve the predicted storm surge in the Salish Sea. It should be noted that the error statistics are based on comparing model results to observations at tide gauges that are primarily in the Main Basin, and therefore wind resolution may be important for modeling storm surge in certain parts of the Salish Sea.

4.3.Model Limitations

The modeling approach used in this study did not consider the contribution of river discharge to storm surge height in the estuaries. Although this approach has been commonly adopted by the storm surge modeling community, it could underestimate the maximum compound surge as a combination of storm surge and river flood near the estuarine mouths in the sub-basins that receive a significant amount of river discharge during the storm events. For instance, the Skagit River and Snohomish River in the Whidbey Basin are both under the threat of frequent river flooding in winter months (Yang et al. 2012, Yang et al. 2015). Hence, the maximum surge height obtained from this study may be underestimated in sub-basins that are heavily influenced by river discharge. Therefore, it is important to simulate the compound flood induced by fluvial and coastal storm surge in future studies because simultaneous occurrence of extreme river discharges and storm surges could exacerbate flood risk (Ikeuchi et al. 2017).

We also chose to force the storm surge model with observed water level time series at the open boundaries. This approach greatly improves the model's accuracy in predicting both astronomical tides and storm surges by reducing the uncertainty associated with open boundary forcing (e.g., remote surge), especially during the storm events. Although this approach is especially suitable for storm surge hindcasting, it may not be sufficient for conducting storm surge forecasting for which the observed open boundary water level information is unavailable. Therefore, expanding the model domain farther outside to cover the coastal Pacific Ocean may provide a useful alternative solution (Shen and Gong 2009, Xu et al. 2010). It also should be pointed out that the observed water level time series at the tidal gauges may also include sea level anomalies that are not necessarily directly associated with the specific storm event being simulated. Hence, the storm surge height obtained from this study should be regarded as the total sea level anomaly that is largely induced by windstorms in the PNW.

5. Conclusions

The PNW coast and the Salish Sea are subject to the threat of storm surge induced by extratropical cyclones. This study presented a systematic modeling assessment of storm surge in the Salish Sea using an unstructured-grid coastal ocean model. A total of 34 major storm surge events during the period from 1980 to 2016 were simulated and model results were validated with observed total water levels and derived storm surge heights at tide gauges located in the Salish Sea. A suite of model performance metrics were calculated to quantify the accuracy of the storm surge simulations. Good error statistics indicate the model has strong skill in reproducing the total water level, storm surge, and current distribution in the Salish Sea.

589 Model results indicate that storm surge varies greatly in the Salish Sea; the largest surge
590 occurs in the Strait of Georgia (1.03 m) and smallest surge in the SJDF (0.83 m) and Main
591 Basin of Puget Sound (0.8 m), which is consistent with the findings of others
592 (Abeysirigunawardena et al. 2011, Soontiens et al. 2016). Storm surge in the Salish Sea is
593 primarily controlled by remote surge induced by extratropical cyclones propagating from the
594 Pacific Ocean, and further amplified in complex sub-basins and modulated by local wind
595 forcing. Because the Salish Sea is dominated by southerly wind in winter months, wind
596 forcing generally results in an increase in storm surge in the northern basin (e.g., Strait of
597 Georgia) and a decrease in storm surge in Puget Sound. However, the contribution of local
598 wind to storm surge height is approximately 20% at the maximum and only a few percentages
599 on average.
600 This study provided a complete picture of the spatial variability of storm surge in the
601 Salish Sea, and elucidated the main forcing mechanisms including remote surge and local
602 wind forcing. Interaction with the complex geometry of sub-basins could also amplify the
603 magnitude of storm surge. Storm surge information generated from this study, especially at
604 the sub-basin scale, is useful for storm surge risk management and mitigation in the Salish
605 Sea. To further improve the model accuracy in simulating storm surge, especially in the
606 estuaries, accurate finer-resolution wind forcing should be considered in future studies.
607 Finally, sensitivity experiments should be carried out to evaluate the effect of other factors,
608 such as bathymetry, river discharge, and the baroclinic effect on the distribution of storm
609 surge.
610
611
612

Acknowledgements

This project was primarily funded by a grant from the NOAA Regional Coastal Resilience Grants Program (grant #NA16NOS4730015). The Puget Sound storm surge model simulation was performed using resources available through Research Computing at Pacific Northwest National Laboratory (PNNL). PNNL is operated by Battelle for the U.S. Department of Energy under Contract DE-AC05-76RL01830.

621 **REFERENCES**

622 Abeysirigunawardena, D.S., Gilleland, E., Bronaugh, D. and Wong, P. (2009) Extreme Wind
623 Regime Responses to Climate Variability and Change in the Inner South Coast of British
624 Columbia, Canada. Atmosphere-Ocean 47(1), 41-62.
625 Abeysirigunawardena, D.S., Smith, D.J. and Taylor, B. (2011) Extreme Sea Surge Responses
626 to Climate Variability in Coastal British Columbia, Canada. Canada. Annals of the
627 Association of American Geographers 101(5), 992-1010.
628 Arns, A., Dangendorf, S., Jensen, J., Talke, S., Bender, J. and Pattiaratchi, C. (2017) Sea-
629 level rise induced amplification of coastal protection design heights. Sci Rep 7, 40171.
630 Babson, A.L., Kawase, A. and MacCready, P. (2006) Seasonal and interannual variability in
631 the circulation of Puget Sound, Washington: A box model study. Atmosphere-Ocean 44(1),
632 29-45.
633 Bilskie, M.V., Hagen, S.C., Alizad, K., Medeiros, S.C., Passeri, D.L., Needham, H.F. and
634 Cox, A. (2016) Dynamic simulation and numerical analysis of hurricane storm surge under
635 sea level rise with geomorphologic changes along the northern Gulf of Mexico. Earths Future
636 4(5), 177-193.
637 Bromirski, P.D., Flick, R.E. and Miller, A.J. (2017) Storm surge along the Pacific coast of
638 North America. Journal of Geophysical Research-Oceans 122(1), 441-457.
639 Chen, C.S., Lai, Z.G., Beardsley, R.C., Sasaki, J., Lin, J., Lin, H.C., Ji, R.B. and Sun, Y.F.
640 (2014) The March 11, 2011 Tahoku M9.0 earthquake-induced tsunami and coastal inundation
641 along the Japanese coast: A model assessment. Progress in Oceanography 123, 84-104.
642 Chen, C.S., Liu, H.D. and Beardsley, R.C. (2003) An unstructured grid, finite-volume, three-
643 dimensional, primitive equations ocean model: Application to coastal ocean and estuaries.
644 Journal of Atmospheric and Oceanic Technology 20(1), 159-186.
645 Cheng, T.K., Hill, D.F. and Read, W. (2015) The Contributions to Storm Tides in Pacific
646 Northwest Estuaries: Tillamook Bay, Oregon, and the December 2007 Storm. Journal of
647 Coastal Research 31(3), 723-734.
648 Eichler, T. and Higgins, W. (2006) Climatology and ENSO-related variability of North
649 American extratropical cyclone activity. Journal of Climate 19(10), 2076-2093.
650 Foreman, M.G.G., Sutherland, G. and Cummins, P.F. (2004) M-2 tidal dissipation around
651 Vancouver Island: an inverse approach. Continental Shelf Research 24(18), 2167-2185.
652 Gao, Y., Leung, L.R., Zhao, C. and Hagos, S. (2017) Sensitivity of US summer precipitation
653 to model resolution and convective parameterizations across gray zone resolutions. Journal of
654 Geophysical Research-Atmospheres 122(5), 2714-2733.
655 Glahn, B., Taylor, A., Kyrkowski, N. and Shaffer, W.A. (2009) The role of the SLOSH
656 model in National Weather Service storm surge forecasting. National Weather Digest 33(1),
657 4-14.
658 Hauer, M.E., Evans, J.M. and Mishra, D.R. (2016) Millions projected to be at risk from sea-
659 level rise in the continental United States. Nature Climate Change 6(7), 691-+.
660 Ikeuchi, H., Hirabayashi, Y., Yamazaki, D., Muis, S., Ward, P.J., Winsemius, H.C., Verlaan,
661 M. and Kanae, S. (2017) Compound simulation of fluvial floods and storm surges in a global
662 coupled river-coast flood model: Model development and its application to 2007 Cyclone
663 Sidr in Bangladesh. Journal of Advances in Modeling Earth Systems 9(4), 1847-1862.
664 Khangaonkar, T., Long, W. and Xu, W.W. (2017) Assessment of circulation and inter-basin
665 transport in the Salish Sea including Johnstone Strait and Discovery Islands pathways. Ocean
666 Modelling 109, 11-32.
667 Large, W.G. and Pond, S. (1981) Open Ocean Momentum Flux Measurements in Moderate
668 to Strong Winds. Journal of Physical Oceanography 11(3), 324-336.

669 Lavelle, J.W., Cokelet, E.D. and Cannon, G.A. (1991) A Model Study of Density Intrusions
670 into and Circulation within a Deep, Silled Estuary - Puget Sound. Journal of Geophysical
671 Research-Oceans 96(C9), 16779-16800.
672 Li, C.Y., White, J.R., Chen, C.S., Lin, H.C., Weeks, E., Galvan, K. and Bargu, S. (2011)
673 Summertime tidal flushing of Barataria Bay: Transports of water and suspended sediments.
674 Journal of Geophysical Research-Oceans 116.
675 Liu, X., Jiang, W.S., Yang, B. and Baugh, J. (2018) Numerical study on factors influencing
676 typhoon-induced storm surge distribution in Zhanjiang Harbor. Estuarine Coastal and Shelf
677 Science 215, 39-51.
678 Martin, J.E., Grauman, R.D. and Marsili, N. (2001) Surface cyclolysis in the North Pacific
679 Ocean. Part I: A synoptic climatology. Monthly Weather Review 129(4), 748-765.
680 Mellor, G.L. and Yamada, T. (1982) Development of a Turbulence Closure-Model for
681 Geophysical Fluid Problems. Reviews of Geophysics 20(4), 851-875.
682 Miller, I.M., Morgan, H., Mauger, G., Newton, T.J., Weldon, R., Schmidt, D., Welch, M. and
683 Grossman, E. (2018) Projected Sea Level Rise for Washington State – A 2018 Assess¬ment.
684 A collaboration of Washington Sea Grant, University of Washington Climate Impacts Group,
685 Oregon State University, University of Washington, and US Geologi¬cal Survey. Prepared
686 for the Washington Coastal Resilience Project., Seattle, Washington, USA.
687 Morey, S.L., Baig, S., Bourassa, M.A., Dukhovskoy, D.S. and O'Brien, J.J. (2006) Remote
688 forcing contribution to storm-induced sea level rise during Hurricane Dennis. Geophysical
689 Research Letters 33(19).
690 Mousavi, M.E., Irish, J.L., Frey, A.E., Olivera, F. and Edge, B.L. (2011) Global warming and
691 hurricanes: the potential impact of hurricane intensification and sea level rise on coastal
692 flooding. Climatic Change 104(3-4), 575-597.
693 Nicholls, R.J. and Cazenave, A. (2010) Sea-level rise and its impact on coastal zones (June,
694 pg 1517, 2007). Science 329(5992), 628-628.
695 Rego, J.L. and Li, C.Y. (2010) Nonlinear terms in storm surge predictions: Effect of tide and
696 shelf geometry with case study from Hurricane Rita. Journal of Geophysical Research-
697 Oceans 115.
698 Saha, S., Moorthi, S., Pan, H.L., Wu, X.R., Wang, J.D., Nadiga, S., Tripp, P., Kistler, R.,
699 Woollen, J., Behringer, D., Liu, H.X., Stokes, D., Grumbine, R., Gayno, G., Wang, J., Hou,
700 Y.T., Chuang, H.Y., Juang, H.M.H., Sela, J., Iredell, M., Treadon, R., Kleist, D., Van Delst,
701 P., Keyser, D., Derber, J., Ek, M., Meng, J., Wei, H.L., Yang, R.Q., Lord, S., Van den Dool,
702 H., Kumar, A., Wang, W.Q., Long, C., Chelliah, M., Xue, Y., Huang, B.Y., Schemm, J.K.,
703 Ebisuzaki, W., Lin, R., Xie, P.P., Chen, M.Y., Zhou, S.T., Higgins, W., Zou, C.Z., Liu, Q.H.,
704 Chen, Y., Han, Y., Cucurull, L., Reynolds, R.W., Rutledge, G. and Goldberg, M. (2010) The
705 Ncep Climate Forecast System Reanalysis. Bulletin of the American Meteorological Society
706 91(8), 1015-1057.
707 Shen, J. and Gong, W.P. (2009) Influence of model domain size, wind directions and Ekman
708 transport on storm surge development inside the Chesapeake Bay: A case study of
709 extratropical cyclone Ernesto, 2006. Journal of Marine Systems 75(1-2), 198-215.
710 Smagorinsky, J. (1963) General circulation experiments with the primitive equations. I. The
711 basic experiment. Monthly Weather Review 91, 99-164.
712 Soontiens, N., Allen, S.E., Latornell, D., Le Souef, K., Machuca, I., Paquin, J.P., Lu, Y.Y.,
713 Thompson, K. and Korabel, V. (2016) Storm Surges in the Strait of Georgia Simulated with a
714 Regional Model. Atmosphere-Ocean 54(1), 1-21.
715 Steenburgh, W.J. and Mass, C.F. (1996) Interaction of an intense extratropical cyclone with
716 coastal orography. Monthly Weather Review 124(7), 1329-1352.

717 Sun, Y.F., Chen, C.S., Beardsley, R.C., Xu, Q.C., Qi, J.H. and Lin, H.C. (2013) Impact of
718 current-wave interaction on storm surge simulation: A case study for Hurricane Bob. Journal
719 of Geophysical Research-Oceans 118(5), 2685-2701.
720 Sutherland, D.A., MacCready, P., Banas, N.S. and Smedstad, L.F. (2011) A Model Study of
721 the Salish Sea Estuarine Circulation. Journal of Physical Oceanography 41(6), 1125-1143.
722 Tebaldi, C., Strauss, B.H. and Zervas, C.E. (2012) Modelling sea level rise impacts on storm
723 surges along US coasts. Environmental Research Letters 7(1).
724 Thomson, R.E., Rabinovich, A.B., Fine, I.V., Sinnott, D.C., McCarthy, A., Sutherland,
725 N.A.S. and Neil, L.K. (2009) Meteorological tsunamis on the coasts of British Columbia and
726 Washington. Physics and Chemistry of the Earth 34(17-18), 971-988.
727 Wang, T.P. and Yang, Z.Q. (2017) A modeling study of tidal energy extraction and the
728 associated impact on tidal circulation in a multi-inlet bay system of Puget Sound. Renewable
729 Energy 114, 204-214.
730 Wang, T.P. and Yang, Z.Q. (2019) The Nonlinear Response of Storm Surge to Sea-Level
731 Rise: A Modeling Approach. Journal of Coastal Research 35(2), 287-294.
732 Wang, T.P., Yang, Z.Q., Wu, W.C. and Grear, M. (2018) A Sensitivity Analysis of the Wind
733 Forcing Effect on the Accuracy of Large-Wave Hindcasting. Journal of Marine Science and
734 Engineering 6(4).
735 Xu, H.Z., Zhang, K.Q., Shen, J.A. and Li, Y.P. (2010) Storm surge simulation along the U.S.
736 East and Gulf Coasts using a multi-scale numerical model approach. Ocean Dynamics 60(6),
737 1597-1619.
738 Yang, Z., García-Medina, G., Wu, W.C., Wang, T., Leung, R., Castrucci, L. and Mauger, G.
739 (2019a) Modeling Analysis of the Swell and Wind-Sea Climate in the Salish Sea. Estuarine,
740 Coastal and Shelf Science Volume 224, 289-300.
741 Yang, Z. and Wang, T. (2013a) Tidal residual eddies and their effect on water exchange in
742 Puget Sound. Ocean Dynamics 63(8), 995-1009.
743 Yang, Z., Wang, T. and Castrucci, L. (2019b) Storm surge modeling in Puget Sound. PNNL
744 Technical Report, PNNL-28685. Pacific Northwest National Laboratory, Richland, WA.
745 https://www.pnnl.gov/main/publications/external/technical_reports/PNNL-28685.pdf.
746 Yang, Z., Wang, T., Khangaonkar, T. and Breithaupt, S. (2012) Integrated modeling of flood
747 flows and tidal hydrodynamics over a coastal floodplain. Environmental Fluid Mechanics
748 12(1), 63-80.
749 Yang, Z.Q. and Khangaonkar, T. (2010) Multi-scale modeling of Puget Sound using an
750 unstructured-grid coastal ocean model: from tide flats to estuaries and coastal waters. Ocean
751 Dynamics 60(6), 1621-1637.
752 Yang, Z.Q., Taraphdar, S., Wang, T.P., Leung, L.R. and Grear, M. (2016) Uncertainty and
753 feasibility of dynamical downscaling for modeling tropical cyclones for storm surge
754 simulation. Natural Hazards 84(2), 1161-1184.
755 Yang, Z.Q. and Wang, T.P. (2013b) Tidal residual eddies and their effect on water exchange
756 in Puget Sound. Ocean Dynamics 63(8), 995-1009.
757 Yang, Z.Q., Wang, T.P., Copping, A. and Geerlofs, S. (2014a) Modeling of in-stream tidal
758 energy development and its potential effects in Tacoma Narrows, Washington, USA. Ocean
759 & Coastal Management 99, 52-62.
760 Yang, Z.Q., Wang, T.P., Leung, R., Hibbard, K., Janetos, T., Kraucunas, I., Rice, J., Preston,
761 B. and Wilbanks, T. (2014b) A modeling study of coastal inundation induced by storm surge,
762 sea-level rise, and subsidence in the Gulf of Mexico. Natural Hazards 71(3), 1771-1794.
763 Yang, Z.Q., Wang, T.P., Voisin, N. and Copping, A. (2015) Estuarine response to river flow
764 and sea-level rise under future climate change and human development. Estuarine Coastal
765 and Shelf Science 156, 19-30.

766 Zhai, L., Greenan, B., Thomson, R. and Tinis, S. (2019) Use of Oceanic Reanalysis to
767 Improve Estimates of Extreme Storm Surge. Journal of Atmospheric and Oceanic
768 Technology.
769 Zhang, H., Cheng, W.C., Qiu, X.X., Feng, X.B. and Gong, W.P. (2017) Tide-surge
770 interaction along the east coast of the Leizhou Peninsula, South China Sea. Continental Shelf
771 Research 142, 32-49.
772 Zhao, L., Chen, C., Vallino, J., Hopkinson, C., Beardsley, R.C., Lin, H. and Lerczak, J.
773 (2010) Wetland-estuarine-shelf interactions in the Plum Island Sound and Merrimack River
774 in the Massachusetts coast. Journal of Geophysical Research 115(C10).
775 Zhong, L.J., Li, M. and Zhang, D.L. (2010) How do uncertainties in hurricane model
776 forecasts affect storm surge predictions in a semi-enclosed bay? Estuarine Coastal and Shelf
777 Science 90(2), 61-72.
778